

Galactic Center Radio Constraints on Gamma-Ray Lines from Dark Matter Annihilation

Ranjan Laha,^{1,2,*} Kenny Chun Yu Ng,^{1,2,†} Basudeb Dasgupta,^{1,‡} and Shunsaku Horiuchi^{1,§}

¹*Center for Cosmology and AstroParticle Physics, Ohio State University,
191 W. Woodruff Ave., Columbus, 43210 OH, USA.*

²*Department of Physics, Ohio State University, 191 W. Woodruff Ave., Columbus, 43210 OH, USA.*

(Dated: May 1, 2022)

Recent evidence for one or more gamma-ray lines at ~ 130 GeV in the Fermi-LAT data from the Galactic Center has been interpreted as a hint for dark matter annihilation to $Z\gamma$ or $H\gamma$ with an annihilation cross section, $\langle\sigma v\rangle \sim 10^{-27}\text{cm}^3\text{s}^{-1}$. We test this hypothesis by comparing synchrotron fluxes due to the electrons and positrons from the decay of the Z and the H boson *only* in the Galactic Center against radio data from the same region. We find that the radio data from single dish telescopes marginally constrain this interpretation of the claimed gamma lines for a contracted NFW profile. Already-operational radio telescopes such as LOFAR, which are sensitive to annihilation cross sections as small as $10^{-28}\text{cm}^3\text{s}^{-1}$, can confirm or rule out this scenario very soon. We discuss the assumptions on the dark matter profile, magnetic fields, and background radiation density profiles, and show that the constraints are relatively robust for any reasonable assumptions. Independent of the above said recent developments, we emphasize that our radio constraints apply to all models where dark matter annihilates to $Z\gamma$ or $H\gamma$.

PACS numbers: 95.35.+d

I. INTRODUCTION

The particle identity of dark matter (DM) is one of the outstanding puzzles in contemporary physics. In order to fully understand the particle properties of dark matter, a number of complementary approaches to dark matter searches have been adopted. Indirect detection of dark matter is a promising technique, in which the products of dark matter annihilation are searched for, and gives us information about the DM abundance and annihilation rate at various astrophysical sites [1–5].

Gamma-ray lines from DM self annihilation are believed to be a smoking-gun signature, and have been investigated in considerable detail [6–11]. Despite the relative freedom in DM model-building, if DM self-annihilation is to two-body Standard Model final states, then gamma-ray line(s) can be produced only via the following three channels (i) $\chi\chi \rightarrow \gamma\gamma$, (ii) $\chi\chi \rightarrow Z\gamma$, and (iii) $\chi\chi \rightarrow H\gamma$, where χ denotes the DM, and Z and H denote the Z and Higgs boson, respectively. We take the Higgs boson to be at 125 GeV [12, 13], and allow a heavier DM to annihilate to it.

Recently, evidence for a gamma-ray line from the Galactic Center (GC) has been uncovered in the Fermi-LAT data at ~ 130 GeV [14, 15] and this has given rise to renewed interest in considering the line signal in more detail [16–31]. The Fermi-LAT collaboration has not confirmed the signal yet [32], as their most recent results have employed a different search strategy, an older data set and background rejection software, and a larger

search region, making it difficult to compare directly with the above claims.

This statistically significant signal has been tentatively interpreted as arising from DM annihilation. Generally speaking, the signal requires a DM self annihilation cross section of $\langle\sigma v\rangle \sim 10^{-27}\text{cm}^3\text{s}^{-1}$ and the Galactic DM halo described by a standard NFW, Einasto, or a contracted NFW profile. Subsequently, a variety of particle physics models have also been proposed to explain the signal [33–52]. It is also found that the line is slightly off-center from the GC [20, 27], which requires that the center of the DM halo to be displaced from the baryonic center. This displacement is also supported by recent simulations [53].

On the other hand, there are arguments against the DM origin of the gamma-ray line. There are hints that the line is also present in the photons collected from the cascades in the Earth’s atmosphere, which is a “pure background” region [20]. Finally, it remains possible that the signal is of an astrophysical origin [17, 54, 55]. Given the arguments in favor of and against the DM origin of this signal, this remains a topic of active research.

More recently, there have been claims of the presence of gamma-ray lines at the same energy, spatially correlated with some Fermi-LAT unassociated sources [24]. However, there are also counterclaims that most of these unassociated sources are consistent with being standard astrophysical objects such as active galactic nuclei or statistical fluctuations [56–58].

If the DM annihilates to two-body Standard Model final states, as in (i)-(iii), then we can predict some particle physics model-independent consequences. For a dominant annihilation (i), i.e., to two photons, there are no further interactions of the photons at an appreciable level, with all higher-level amplitudes suppressed by at least $\alpha \approx 1/137$. However, if the annihilation proceeds

* laha.1@osu.edu

† ng.199@osu.edu

‡ dasgupta.10@osu.edu

§ horiiuchi@mps.ohio-state.edu

as in (ii) or (iii), i.e., to a photon and a heavy Standard Model boson, the heavy boson decays to other charged particles which can have observable consequences.

The decay of the Z and the H boson produces electrons, protons, neutrons, neutrinos, their antiparticles, as well as photons as final states. The almost featureless spectra of these secondary particles poses considerable difficulty in their search above the astrophysical backgrounds. Searches for antimatter benefit from lower cosmic ray backgrounds, therefore one can search for antiprotons and positrons from the Z and the H boson. A search for antiprotons from these decays constrains several particle physics models which can give rise to a gamma-ray line [21], whereas the preexisting unaccounted excess in positrons [59, 60] makes a positron search ambiguous. Neutrinos could, in principle, be used to distinguish between all three final states, but achieved or projected sensitivities in the range $\langle\sigma v\rangle \sim (10^{-22} \text{ cm}^3 \text{ s}^{-1} - 10^{-23} \text{ cm}^3 \text{ s}^{-1})$ [61–64] will not be able to probe the claimed signal. Secondary photons that are produced in the decay of the Z and the H boson, or in other DM annihilation channels, also constrain these scenarios [21–23], and there are ongoing efforts to confirm this 130 GeV line with future detectors [25, 30].

In this paper, we ask the questions – If the 130 GeV signal is indeed from DM annihilation to $Z\gamma$ or $H\gamma$, what other consequences are guaranteed? Can we use these consequences to test this signal? Synchrotron radiation from products of DM annihilation has been argued to provide strong constraints for many DM annihilation channels and scenarios [65–81]. Thus, following these promising leads, we explore our question by calculating the synchrotron radiation in the GC due to the electrons and positrons from Z and H decays *only*, and comparing it to existing data from radio telescopes.

We first take a very conservative approach, where we compare the DM-induced synchrotron fluxes to the total measured radio flux at 330 MHz in a relatively large region around the GC, and determine that DM annihilation cross sections to these channels cannot be more than $\langle\sigma v\rangle \sim 10^{-25} \text{ cm}^3 \text{ s}^{-1}$. However, this approach is overly conservative, as the synchrotron fluxes in the GC are modeled accurately with known astrophysics. We argue that the flux due to dark matter must not exceed the uncertainties on the modeled radio fluxes, which provides us with a constraint $\langle\sigma v\rangle \lesssim 10^{-26} \text{ cm}^3 \text{ s}^{-1}$. Constraints obtained by comparing fluxes predicted in smaller regions of interest and upper limits at 408 MHz imply $\langle\sigma v\rangle \sim 10^{-27} \text{ cm}^3 \text{ s}^{-1}$, and are already in mild tension with the 130 GeV line. We forecast that the sensitivity can be improved to $\sim 10^{-28} \text{ cm}^3 \text{ s}^{-1}$ with a few hours of observation of the GC at 200 MHz with LOFAR, the LOw-Frequency ARray for radio astronomy, allowing us to constrain interpretations of the 130 GeV line signal in the Fermi-LAT data in terms of DM annihilation to $Z\gamma$ or $H\gamma$. Although this is the main motivation for our present work, the radio constraints we derive are valid regardless of whether this claimed 130 GeV line signal

survives further scrutiny or not. These constraints will continue to apply to any future interpretations of gamma-ray lines at the GC in terms of DM annihilation.

Note that, these sensitivities readily probe the cross section that explains the tentative 130 GeV line signal. More generally, we expect these sensitivities to be able to probe many of the models [40, 46], not necessarily supersymmetric, that could explain this signal. We also emphasize that since we are looking for the synchrotron radiation from the electrons and positrons produced in the decays of the Z and the H boson *only*, our constraints are independent of the underlying DM particle physics model. In these two ways, our work is complementary to Ref. [22]. The results here are of course affected by astrophysical uncertainties, e.g., dark matter density profile, magnetic fields, interstellar radiation energy density, and proton density in the Galaxy, and by taking a range of different values for them we try to understand their impact.

The rest of the paper is organized as follows. In Sec. II we discuss the radio data that we use for obtaining our constraints, and the theoretical framework for calculating the flux densities from synchrotron radiation by DM annihilation products. In Sec. III we furnish and justify the astrophysical inputs, i.e., DM density, magnetic fields, and radiation density in the Galaxy, that we use for our calculations. In Sec. IV we show the predicted flux densities for benchmark DM annihilation cross sections, and provide constraints on the DM annihilation cross section as a function of DM mass for the channels $\chi\chi \rightarrow Z\gamma$ and $\chi\chi \rightarrow H\gamma$, and conclude in Sec. V.

II. EXPERIMENTAL DATA AND THEORETICAL FRAMEWORK

A. Radio data and regions of interest

We use radio data at two frequencies, 330 MHz and 408 MHz, to obtain the limits on DM self annihilation cross section from current radio observations near the GC. We also use the projected radio sensitivity by the LOFAR telescope at 200 MHz [82] to predict the future sensitivity on DM self annihilation cross section to gamma-ray lines that can be probed by radio data.

1. ROI-2°: Region of interest 2° around GC

The radio measurements in the 330 MHz band by the Green Bank telescope are available in a $6^\circ \times 2^\circ$ region around the GC [83], and provides us our first region of interest (ROI-2°). This region is fairly large, and our calculation of the radio fluxes are unaffected by the uncertainties in the dark matter density profile at small radii, but more affected by the uncertainties in magnetic fields. We approximate this region to be a circle with a radius 0.034 radians ($\approx 2^\circ$), for simplicity. Thus, we

match the area of the region of observation in [83], but the shape is different. We assume that this difference will not change our results significantly. In [83], the authors present an astrophysical model to explain the data, so we use the uncertainty in their measurement at 330 MHz, i.e., $0.05 \times 18000 \text{ Jy} = 900 \text{ Jy}$, to obtain our limits on the self annihilation cross section as a function of the DM mass. The authors in [83] also use radio data at higher frequencies to construct a GC model. Comparing our calculated synchrotron flux density with the errors in their measurement at every measured frequency we find that the most constraining limit on DM self annihilation cross section comes from the lowest frequency band (330 MHz) and hence we only use the uncertainty in the measurement at 330 MHz to constrain DM properties. We do not consider the measurement at 74 MHz to obtain our limits, as absorption and scattering are problematic at these low frequencies near the GC.

2. ROI-4'': Region of interest 4'' around GC

The radio measurement in the 408 MHz band by the Jodrell Bank telescope [84] in a region 4'' around the GC provides us with our second region of interest (ROI-4''). At this frequency, the region of interest is a circle of angular radius 4'' and the upper limit on the radio flux is 50 mJy. This region is significantly smaller, and affected more strongly by the uncertainties in the DM density profile and the detailed modeling of the magnetic fields near the GC black hole.

Finally, anticipating future radio measurements near the GC [82], we also estimate the constraints that can be obtained on DM self annihilation channels that produce a gamma-ray line using the projected sensitivity of LOFAR. From the information presented in [82], we deduce that LOFAR can reach a sensitivity of 3.2 mJy for a 4'' radius around the GC at 200 MHz for 6 hours of observation of the GC. If it is found that the actual synchrotron flux near the GC is larger, one can then model the synchrotron flux due to expected astrophysical processes and then use the uncertainty in that measurement to constrain the DM particle properties (as we have done for the 330 MHz band). For simplicity, we assume that a sensitivity of 3.2 mJy in this region around the GC will be reached, and forecast constraints accordingly.

B. Theoretical framework

To calculate the synchrotron flux from DM self annihilation products, in principle, we need to solve the time-independent diffusion equation for the produced electrons and positrons [68]

$$K(E)\nabla^2 n_e(E, \mathbf{r}) + \frac{\partial}{\partial E} [b(E, \mathbf{r})n_e(E, \mathbf{r})] = -S(E, \mathbf{r}), \quad (1)$$

where $n_e(E, \mathbf{r})$ is the electron density spectrum per unit energy interval, $K(E)$ is the diffusion coefficient, $b(E, \mathbf{r})$ is the energy-loss rate and $S(E, \mathbf{r})$ is the source injection spectrum of the electrons. Here E denotes the energy of the electron and \mathbf{r} denotes the position of the electron.

For ROI-2'', it can be shown that we are in a regime where the GeV electrons will travel only $\sim 30 \text{ pc}$ [70, 85] during their cooling lifetime. Since this length is much smaller than the length associated with ROI-2'', we conclude that diffusion will have a small impact on our results. For ROI-4'', due to the presence of very high magnetic fields near the GC (see Sec. III B - Magnetic fields), and consequently high energy loss rates, the diffusion length $\langle l(E) \rangle \sim \sqrt{KE/b}$, is very small and diffusion can be safely neglected. However, for increased precision, one may in future improve our results by performing a more detailed numerical study along the lines of [81].

These electrons and positrons then lose energy via the synchrotron process, the inverse Compton process, and the bremsstrahlung process. For our purposes, the total energy loss rate is given by

$$b(E, \mathbf{r}) = b_{\text{sync}}(E, \mathbf{r}) + b_{\text{IC}}(E, \mathbf{r}) + b_{\text{brem}}(E, \mathbf{r}). \quad (2)$$

Ionization energy loss is important for electrons and positrons only at lower energies than are considered in this work.

Synchrotron energy losses are due to the interaction of the electron and the positron with the Galactic magnetic field. The energy loss rate due to synchrotron process is given by (all formulae in this section are in SI units) [68]

$$\begin{aligned} \left. \frac{dE}{dt} \right|_{\text{sync}} &= \frac{4}{3} \sigma_T c U_{\text{mag}}(\mathbf{r}) \gamma^2 \beta^2 \\ &= 3.4 \times 10^{-17} \text{ GeV s}^{-1} \left(\frac{E}{\text{GeV}} \right)^2 \left(\frac{B(\mathbf{r})}{3 \mu\text{G}} \right)^2, \end{aligned} \quad (3)$$

where $\sigma_T = e^4/(6\pi\epsilon_0^2 m_e^2 c^4)$ is the Thompson scattering cross section [86], U_{mag} is the magnetic energy density, $\gamma = E/m_e$ is the Lorentz factor, and $\beta = \sqrt{\gamma^2 - 1}/\gamma$. The photons emitted because of synchrotron energy loss is generally in the radio band.

Inverse Compton energy losses are caused by the up-scattering of the photons in the GC region (which is mainly composed of the CMB and the background starlight) by the more energetic electrons and the positrons. The energy loss rate due to the inverse Compton process is given by [68]

$$\begin{aligned} \left. \frac{dE}{dt} \right|_{\text{IC}} &= \frac{2}{9} \frac{e^4 U_{\text{rad}}(\mathbf{r}) E^2}{\pi \epsilon_0^2 m_e^2 c^7} \\ &= 10^{-16} \text{ GeV s}^{-1} \left(\frac{E}{\text{GeV}} \right)^2 \left(\frac{U_{\text{rad}}(\mathbf{r})}{\text{eV cm}^{-3}} \right), \end{aligned} \quad (4)$$

where U_{rad} is the radiation energy density. The photons from the CMB and the background starlight is generally up scattered to gamma-ray energies by the energetic

electrons and positrons from the decays of the Z -boson and the Higgs boson.

Bremsstrahlung losses are caused by the emission of gamma-ray photons by the electrons and positrons due to their interaction with the nuclei in the Galaxy. The energy loss rate for this process is given by the Bethe-Heitler formula [87]. We assume that the hydrogen are the dominant nuclei present in the Galaxy. The energy loss rate due to bremsstrahlung is given by

$$\left. \frac{dE}{dt} \right|_{\text{brem}} = 3 \times 10^{-15} \text{ GeV s}^{-1} \left(\frac{E}{\text{GeV}} \right) \left(\frac{n_{\text{H}}}{3 \text{ cm}^{-3}} \right), \quad (5)$$

where we use $n_{\text{H}} \approx 3 \text{ cm}^{-3}$ as the number density of hydrogen nuclei in the interstellar matter in the Galaxy.

The source term is due to the particle injection from DM self annihilation

$$S(E, \mathbf{r}) = \frac{1}{2} \langle \sigma v \rangle \left(\frac{\rho_{\chi}(\mathbf{r})}{m_{\chi}} \right)^2 \frac{dN_e}{dE}, \quad (6)$$

where m_{χ} denotes the mass of the DM particle, $\rho_{\chi}(\mathbf{r})$ denotes the DM density distribution. dN_e/dE denotes the number of electrons and positrons from the decay of the Z or the H boson per unit energy interval, which we calculate using PYTHIA [88].

Collecting the above mentioned inputs and in the no diffusion limit [70], we can write electron density spectrum per unit energy interval as

$$n_e(E, \mathbf{r}) = - \frac{\int_E^{m_{\chi}} dE' S(E', \mathbf{r})}{b(E, \mathbf{r})}. \quad (7)$$

1. Flux density in ROI-2°

The synchrotron power density per unit frequency from a spectrum of electrons and positrons is given by [87, 89]

$$L_{\nu}(\mathbf{r}) = \int dE n_e(E, \mathbf{r}) \times \left\{ \frac{1}{4\pi\epsilon_0} \frac{\sqrt{3}e^3 B(\mathbf{r})}{m_e c} \left(\frac{\nu}{\nu_c} \int_{\nu/\nu_c}^{\infty} dx K_{5/3}(x) \right) \right\}, \quad (8)$$

where the critical frequency, ν_c , is given by

$$\nu_c = \frac{3eE^2 B}{4\pi m_e^3 c^4} = 16 \text{ MHz} \left(\frac{E}{\text{GeV}} \right)^2 \left(\frac{B}{\mu\text{G}} \right), \quad (9)$$

and $K_{5/3}(x)$ denotes the modified Bessel function of order $5/3$.

The synchrotron radiation flux density is given by

$$F_{\nu} = \frac{1}{4\pi} \int d\Omega \int dl L_{\nu}(\mathbf{r}), \quad (10)$$

where l denotes the line of sight distance and Ω is the angular area of the region of interest.

We have verified that the synchrotron self-absorption is unimportant for these parameters which is generally a

problem near the GC at frequencies below approximately 100 MHz [82].

2. Flux density in ROI-4''

For the smaller region of interest of radius $4''$ around the GC, i.e., ROI-4'', we follow the method presented in [67], which is dependent on the morphology of the magnetic field near the GC black hole. Due to the strong magnetic fields in this region, we assume that the energy loss of the electron is dominated by the synchrotron energy losses. In this case, we approximate

$$\frac{\nu}{\nu_c} \int_{\nu/\nu_c}^{\infty} dx K_{5/3}(x) \approx \frac{8\pi}{9\sqrt{3}} \delta \left(\frac{\nu}{\nu_c} - \frac{1}{3} \right). \quad (11)$$

The synchrotron flux density in this case is given by [67]

$$F_{\nu} = \frac{1}{4\pi(8.5 \text{ kpc})^2} \frac{\langle \sigma v \rangle}{2m_{\chi}^2} \int dV \rho_{\chi}^2 E \int_E^{m_{\chi}} \frac{dN}{dE'} dE', \quad (12)$$

where the first integral is over the volume of observation and the second integral counts the number of particles above a certain energy E . The value of E in this case can be found by using Eqs. (9) and (11) and is given by

$$E = 433 \text{ MeV} \sqrt{\left(\frac{\nu}{\text{MHz}} \right) \left(\frac{\mu\text{G}}{B} \right)}. \quad (13)$$

III. ASTROPHYSICAL INPUTS FOR CALCULATIONS

A. DM density profiles

One of the major unknowns near the GC is the DM density profile. Almost all simulations agree on the radial dependence of the DM density profile at large radii from the GC, $\rho(r) \sim r^{-3}$. However, due to limited numerical resolution and the complicated astrophysics at the GC, the simulations disagree on the shape of the density profile at small radii.

Observations of elliptical galaxies [90], early-type galaxies [91], M31 [92], and M84 [93] prefer a cuspy profile [94] in contrast to dwarf galaxies which prefer a cored profile [95]. Given that M31 is a Milky Way like galaxy, we assume that the DM density profile in the Milky Way is not cored and hence we do not consider the cored isothermal profile in our work. In general, the constraints from the indirect detection searches are especially weak for a cored isothermal profile [67, 70].

In this work, we use three different DM profiles which provide reasonable constraints from the radio measurements at the GC. The dark matter density at the solar radius has a value of $0.3 \pm 0.1 \text{ GeV/cm}^3$ [96]. For concreteness, in this work, we take the benchmark value

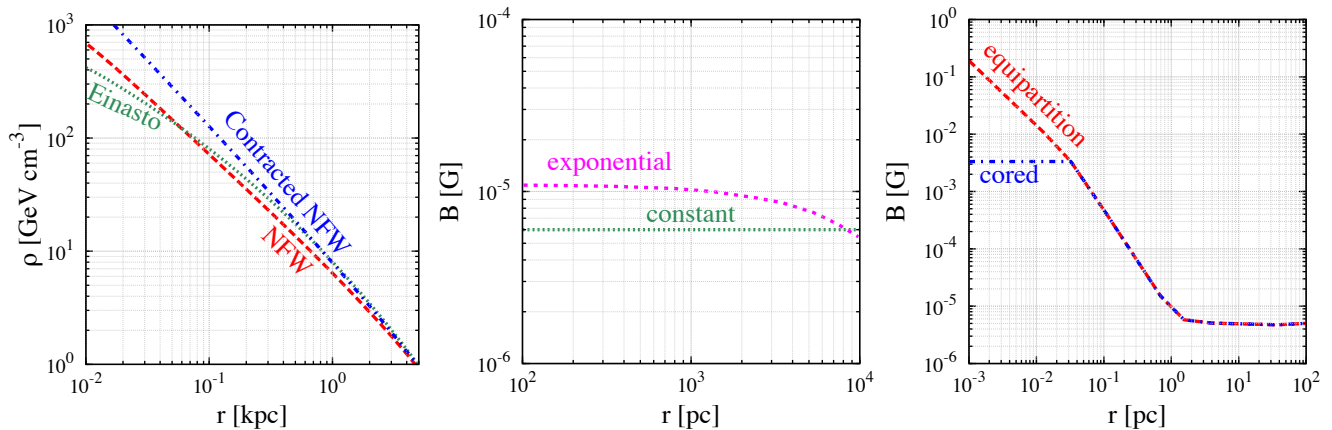


FIG. 1. Galactic dark matter density (left panel) and magnetic field profiles (middle and right panels). **(Left)** We show the various DM profiles used in this work: the Einasto profile (14), the NFW profile (15) and the contracted NFW profile (16). **(Middle)** We show the magnetic field used for calculating the synchrotron flux in ROI-2°, i.e., a region of angular radius 2° around the GC. The constant magnetic field has a value of 6 μG everywhere in the Galaxy. The exponential magnetic field is given in Eq. (17) and has a value of 6 μG at the solar radius. **(Right)** We show the magnetic field used for calculating the synchrotron flux in ROI-4'', i.e., in a region of angular radius 4'' around the GC. The “equipartition” magnetic field is given by Eq. (18) and the “cored” magnetic field is given by Eq. (20). Both the fields have been normalized to have a value of 6 μG at the solar radius.

to be 0.4 GeV/cm³ [97, 98]. Note that local dark matter density taken in the papers which discuss the presence of the 130 GeV line at the GC is also 0.4 GeV/cm³ (see for e.g., [14, 16]).

The Einasto dark matter profile [99–102],

$$\rho_{\text{Ein}}(r) = \frac{0.08 \text{ GeV cm}^{-3}}{\exp\left[\frac{2}{0.17} \left(\left(\frac{r}{20 \text{ kpc}}\right)^{0.17} - 1\right)\right]}. \quad (14)$$

is the least cuspy of all the DM profiles considered in this work, and hence we expect this profile to produce least amount of synchrotron radiation, especially when we consider the synchrotron radiation from a region very near the GC.

We then consider the standard NFW profile [103]

$$\rho_{\text{NFW}}(r) = \frac{0.35 \text{ GeV cm}^{-3}}{\left(\frac{r}{20 \text{ kpc}}\right) \left(1 + \frac{r}{20 \text{ kpc}}\right)^2}. \quad (15)$$

The cuspy nature of this DM density profile will ensure that we get a larger synchrotron radiation flux than what we expect from the Einasto profile when we consider observation from a region very near to the GC.

We finally consider a contracted NFW profile

$$\rho_{\text{con. NFW}}(r) = \frac{0.29 \text{ GeV cm}^{-3}}{\left(\frac{r}{20 \text{ kpc}}\right)^{1.15} \left(1 + \frac{r}{20 \text{ kpc}}\right)^{1.85}}. \quad (16)$$

The steeper inner slope in this case can be due to either a GC black hole [104], or due to adiabatic contraction due to the presence of baryonic matter at the GC [105–108],

which have been supported by more recent numerical simulations [94]. The inner slope of the DM profile obeys the complementary constraints presented in [109].

These DM profiles are shown in the left panel in Fig. 1. It is evident from the figure that, at small radii, the contracted NFW profile has the steepest slope, and the Einasto profile has the shallowest slope of all the three DM profiles considered in this work. From the figure, one can also infer that the DM density profiles have almost the same shape at large distances from the GC.

B. Magnetic fields

The GC magnetic field has both a regular and a turbulent component. For both the components, the normalization and the radial profile is not understood very well. In particular, the magnetic field amplitude near the GC is uncertain, with measured estimates spanning a range of some two orders of magnitude between 10 μG [110] and 10³ μG on scales of a few ~ 100 pc [111]. In order to account for the uncertainty in the magnetic field, we adopt several configurations. In all cases, we initially fix the normalization to a value $B_{\odot} = 6 \mu\text{G}$ at the solar system radius ($r_{\odot} = 8.5 \text{ kpc}$). This is mid-range among the various estimates of B_{\odot} which span between 3 μG and 10 μG [112–114]. We will discuss how our results scale with the different values of B_{\odot} when we present our results.

1. Magnetic fields in ROI-2°

For ROI-2°, i.e., a circular region with radius 2° around the GC (distance scale ~ 200 pc for $r_\odot = 8.5$ kpc), we consider two different magnetic field radial profiles. The first is the spherically symmetric exponential profile,

$$B(r) = B_\odot \exp\left(-\frac{r - r_\odot}{R_m}\right), \quad (17)$$

where r is the distance from the GC, and $R_m = 14$ kpc is the scale radius. Our choice of R_m follows from Ref. [69], where we adopt their Galactic magnetic field model ‘‘GMF I’’ and their best-fit propagation parameters. We add that we neglect the z -dependence of the magnetic field which is only weakly constrained by data and remain highly uncertain. Using this conservative magnetic field, the magnetic field at a radius of 2° is $\approx 11 \mu\text{G}$. Although this value is within the range of estimates of the magnetic field in the GC, it is closer to the lower range. In addition, it does not obey the lower limit of $50 \mu\text{G}$ on scales of 400 pc presented in [83]. However, given the uncertainties in the astrophysical and propagation quantities, we do not consider this difference significant. For example, if we adopt instead $B_\odot = 10 \mu\text{G}$ and the ‘‘MAX’’ propagation parameters of [69], we obtain $R_m \approx 8.5$ kpc and a magnetic field at 2° of $\approx 27 \mu\text{G}$. To estimate the impact of the normalization of the magnetic field, we will also show our results for two extreme values for B_\odot , i.e., $3 \mu\text{G}$ and $10 \mu\text{G}$.

To estimate the uncertainty due to the shape of the magnetic field profile we also adopt the extreme case of a constant magnetic field of value B_\odot everywhere [73]. Both of these are shown on the middle panel of Figure 1.

2. Magnetic fields in ROI-4’’

For ROI-4’’, i.e., a region with radius 4’’ around the GC (distance scale ~ 0.2 pc for $r_\odot = 8.5$ kpc), we need to take into account the influence of the supermassive black hole (SMBH) at the GC. The presence of the SMBH sets two length-scales: the Schwarzschild radius, $R_{\text{BH}} \approx 1.2 \times 10^{12} (M/4.3 \times 10^6 M_\odot)$ cm, and the radius $R_{\text{acc}} \approx 0.04$ pc within which the free-fall velocity due to the gravity of the SMBH $v = -c\sqrt{R_{\text{BH}}/r}$ is larger than the random Galactic motion, $\sim 10^{-3}c$. In other words, the region $r < R_{\text{acc}}$ defines the accretion region.

We adopt the ‘‘equipartition model’’ for the Galactic magnetic field, described by various authors [e.g., 67]. In this model, the SMBH accretes matter from a radius of R_{acc} , and the magnetic field in the accretion flow achieves its equipartition with the kinetic pressure, i.e., $B^2(r)/(2\mu_0) = \rho(r)v^2(r)/2$. For a constant mass accretion rate, \dot{M} , one obtains $\rho(r) = \dot{M}/4\pi r^2 v(r) \propto r^{-3/2}$, and thus $B(r) \propto r^{-5/4}$. Outside of R_{acc} , the conservation of magnetic flux is assumed, yielding $B(r) \propto r^{-2}$.

Thus, the equipartition magnetic field is given by

$$B_{\text{eq}}(r) = \begin{cases} B_{\text{acc}}(r/R_{\text{acc}})^{-5/4} & r \leq R_{\text{acc}} \\ B_{\text{acc}}(r/R_{\text{acc}})^{-2} & R_{\text{acc}} < r \leq R_{\text{flux}} \\ B_\odot & R_{\text{flux}} < r, \end{cases} \quad (18)$$

where $R_{\text{acc}} \approx 0.04$ pc, $R_{\text{flux}} \sim 100 R_{\text{acc}}$, and

$$B_{\text{acc}} = 7.9 \text{ mG} \left(\frac{M_{\text{BH}}}{4.3 \times 10^6 M_\odot} \right)^{1/4} \left(\frac{\dot{M}}{10^{22} \text{ g/s}} \right), \quad (19)$$

for typical values of B_\odot .

We also consider a variant of the equipartition model, where the inner magnetic field is kept smaller because equipartition is prevented somehow. This may occur if, for example, magnetic field dissipation occurs by reconnection in the turbulent accretion flow (see, e.g., [115] and references therein). Since the details of dissipation are not well understood, we conservatively adopt a constant magnetic field throughout the accretion region, namely,

$$B_{\text{cored}}(r) = \begin{cases} B_{\text{acc}} & r \leq R_{\text{acc}} \\ B_{\text{acc}}(r/R_{\text{acc}})^{-2} & R_{\text{acc}} < r \leq R_{\text{flux}} \\ B_\odot & R_{\text{flux}} < r. \end{cases} \quad (20)$$

We call this the cored magnetic field. These are shown on the right panel of Figure 1.

C. Radiation energy density

The radiation energy density is the sum of the energy density of the CMB photons and the energy density of the background starlight photons. The energy density of the CMB photons is 0.3 eV cm^{-3} . The radiation energy density due to the background starlight varies with position in the Galaxy from 1 eV cm^{-3} to 10 eV cm^{-3} . Conservatively, we take the background starlight energy density to have a constant value of 9 eV cm^{-3} . Hence we use the total radiation field energy density as $U_{\text{rad}} = 9 \text{ eV cm}^{-3}$ in this work. We also check our results by taking a much smaller radiation energy density of 0.9 eV/cm^3 and find that using this lower value of the radiation field energy density improves our constraints by a factor of $\sim 2 - 3$.

IV. RESULTS

In this section, we first present our results for the synchrotron fluxes from DM annihilation products, and discuss the expected systematic uncertainty due to incomplete knowledge of the DM and magnetic field profiles. We then compare the expected flux with available/projected radio data from the GC to arrive at constraints/sensitivities on the DM annihilation cross section. We perform this exercise for three frequency

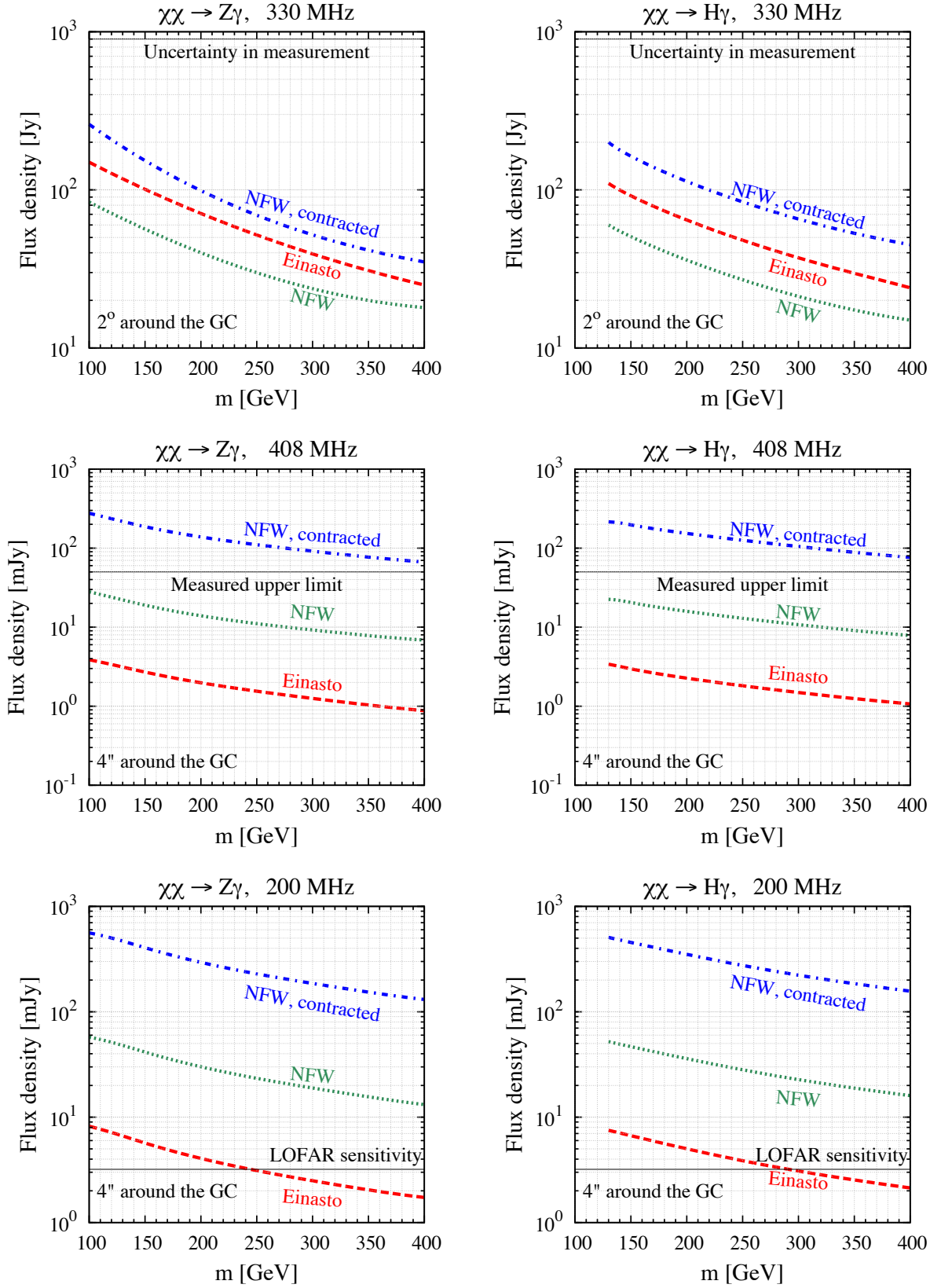


FIG. 2. Prediction of the synchrotron flux density against mass of the DM. In all the plots, we set as a benchmark DM annihilation cross section $\langle\sigma v\rangle = 10^{-26} \text{ cm}^3 \text{ s}^{-1}$, and consider three different DM profiles: Einasto profile in Eq. (14), NFW profile in Eq. (15) and the contracted NFW profile in Eq. (16). **(Left)** $\chi\chi \rightarrow Z\gamma$. **(Right)** $\chi\chi \rightarrow H\gamma$. **(Top)** Results for 330 MHz using the exponential magnetic field in Eq. (17). We also show the uncertainty in the measurement which is used to derive our constraints in this frequency band. **(Middle)** Results for 408 MHz using the equipartition magnetic fields in Eq. (18). We also show the upper limit of the measurement which is used to derive our constraints in this frequency band. **(Bottom)** Results for 200 MHz using the equipartition magnetic fields in Eq. (18). We also show the sensitivity of LOFAR which is used to derive our constraints in this frequency band. The region of interest is specified in the lower left hand corner of each panel.

bands (330 MHz, 408 MHz, and 200 MHz) in two different regions of interest around the GC.

A. Synchrotron flux density at the GC

1. Flux density at 330 MHz

We calculated the synchrotron flux according to the prescription and inputs presented in Sec. III and plot, in the top panel of Fig. 2, the flux density due to synchrotron radiation from DM self annihilation products against mass of the DM for a region of radius 2° around the GC in 330 MHz radio band. The magnetic field used for the top row is a spherically symmetric exponential magnetic field, taken from Eq. (17) with the magnetic field at the solar radius normalized to be $6 \mu\text{G}$. We assume the self annihilation channel to be $\chi\chi \rightarrow Z\gamma$ or $\chi\chi \rightarrow H\gamma$, and for both we assume a benchmark self annihilation cross section $\langle\sigma v\rangle = 10^{-26} \text{ cm}^3 \text{ s}^{-1}$. The uncertainty in the measurement of the synchrotron flux density in this region around the GC at this frequency band, 900 Jy [83], is also shown in the plot and is used to obtain our constraints on the DM particle properties.

The synchrotron flux from DM annihilation products is maximum for the contracted NFW profile. This is easy to understand because the signal is proportional to ρ^2 and a larger ρ increases the signal at the GC. When the region of interest is fairly large, e.g., ROI- 2° , the Einasto profile is predicted to lead to more annihilation than the standard NFW profile. At such a large distance from the GC, the synchrotron energy density only varies by a factor of a few for different DM profiles, demonstrating the relative robustness of these results.

2. Flux density at 408 MHz

We calculated the flux densities as in the previous case, and plot it vs. the mass of the DM in the middle row in Fig. 2. We assume a benchmark self annihilation cross section $\langle\sigma v\rangle = 10^{-26} \text{ cm}^3 \text{ s}^{-1}$. The changes are that the region of interest is now a circular region of radius $4''$ around the GC and the frequency of radio observations is taken to be 408 MHz. The magnetic field used in the second row of Fig. 2 is an equipartition magnetic field, taken from Eq. (18). We get very similar results (differences of less than 1 mJy) if we use the cored magnetic field, as given in Eq. (20). A different value of the magnetic field at the solar radius (within the range $3 \mu\text{G}$ to $10 \mu\text{G}$) does not change the value of the synchrotron flux density by more than a factor of two. The upper limit on the synchrotron flux density in this region around the GC at this frequency, 50 mJy [84], is also shown in the plot and is used to obtain our constraints on the DM particle properties.

As expected, the synchrotron flux from DM annihilation products is maximum for the contracted NFW

profile. However, in contrast to the above we find that for smaller regions of interest, e.g., ROI- $4''$ the cuspleness of NFW profile at lower radii leads to larger fluxes than from the Einasto profile. Note however, that for such small regions of interest around the GC, the flux varies by orders of magnitude for the different DM profiles.

3. Flux density at 200 MHz

Encouraged by the capabilities of the low frequency radio telescope LOFAR, we look at the flux predictions at a frequency of 200 MHz. Note that LOFAR is capable of observing at much lower frequencies but, due to absorptions, the radio sky can be opaque near the GC at frequencies $\lesssim 100$ MHz. However, the 200 MHz band is well above the frequencies at which those absorption effects kick in. As an aside we would like to emphasize that there exists patches of the sky near the GC that are visible even below 100 MHz [82], which maybe interesting regions for DM probes in the future. The projected LOFAR sensitivity at this region around the GC in this frequency band, 3.2 mJy [82], is also shown in the plot and is used to obtain our constraints on the DM particle properties.

We plot the flux density from DM self annihilation products vs. the mass of the DM in the bottom row of Fig. 2. We again assume a benchmark self annihilation cross section $\langle\sigma v\rangle = 10^{-26} \text{ cm}^3 \text{ s}^{-1}$. The region of interest is taken to be a circular region of radius $4''$ around the GC and the frequency of radio observation is taken to be 200 MHz. The magnetic field used is again, the equipartition magnetic field, taken from Eq. (18). At such a small scales around the GC, the flux varies by orders of magnitude for different DM profiles.

B. Sensitivity to magnetic fields

Now, we explore the sensitivity of the predicted synchrotron fluxes to the normalization and shape of the Galactic magnetic field profile. We remind the reader that we have used $6 \mu\text{G}$ as our benchmark value of the magnetic field at the solar radius for all our calculations. The DM is assumed to have a standard NFW profile (Eq. 15) for all the figures here.

To understand the impact of the normalization of the Galactic magnetic field on the synchrotron flux density due to dark matter annihilation, in Fig. 3 we plot the synchrotron flux due to two different values of the Galactic magnetic field at the solar radius: $3 \mu\text{G}$ and $10 \mu\text{G}$. It is seen that varying the normalization of the Galactic magnetic field can change the synchrotron flux density by a factor of a few for both the exponential magnetic field profile and the constant magnetic field profile.

We then show the impact of two different magnetic field profiles: the exponential profile, Eq. (17), and the

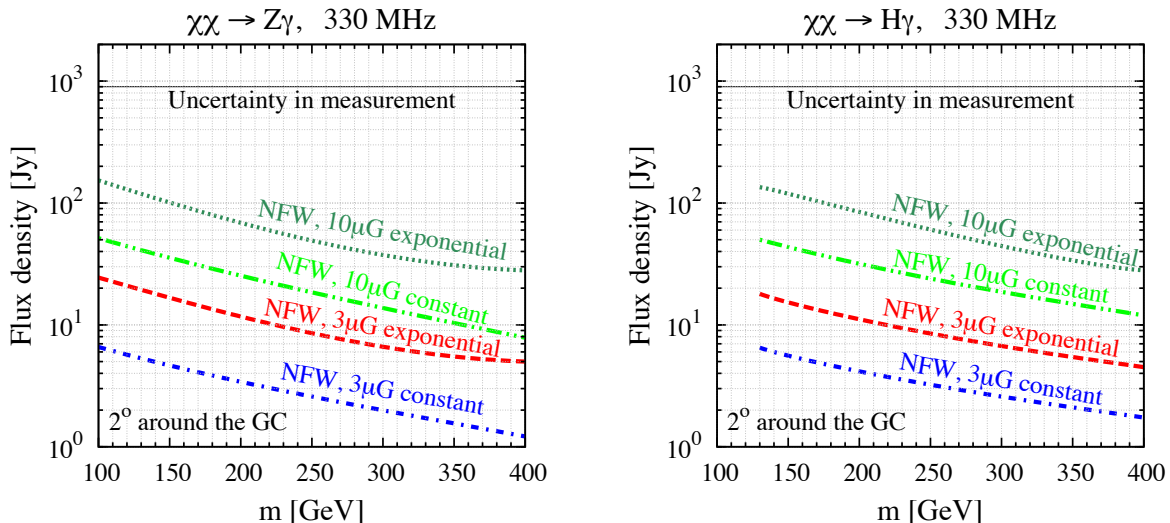


FIG. 3. Prediction of the synchrotron flux density vs. mass of the DM for different annihilation channels at 330 MHz, in a region 2° around the GC. The magnetic field used is exponential, as in Eq. (17), and we use two different values of the magnetic fields at the solar radius: $3 \mu\text{G}$ and $10 \mu\text{G}$. We also show the results for a constant magnetic field profile normalized to $3 \mu\text{G}$ or $10 \mu\text{G}$ inside the Galaxy. For all the panels, we have taken $\langle\sigma v\rangle = 10^{-26} \text{cm}^3 \text{s}^{-1}$ and the NFW profile in Eq. (15). (Left) $\chi\chi \rightarrow Z\gamma$. (Right) $\chi\chi \rightarrow H\gamma$. We also show the uncertainty in the measurement in this band. The region of interest is specified in the lower left hand corner of each panel.

constant magnetic field profile for the 330 MHz band. For a given normalization of the magnetic field profile at the solar radius, we see that the flux due to the exponential magnetic field profile is always larger than the flux due to the constant magnetic field profile for both the DM annihilation channels, $\chi\chi \rightarrow Z\gamma$ and $\chi\chi \rightarrow H\gamma$.

The overall uncertainty in the normalization and the shape of the Galactic magnetic field can lead to a difference of at most an order of magnitude in the predicted synchrotron flux in the 2° around the GC at 330 MHz. We have checked that the variation in the synchrotron flux density with the normalization and shape of the Galactic magnetic field is similar for the other DM profiles considered in this work.

For the region of angular radius $4''$ around the Galactic Center, the difference in the synchrotron flux density is less than a factor of two for both the equipartition, Eqn.(18) and the cored magnetic field profile, Eqn.(20), for a given DM profile. Again, the uncertainty due to incomplete knowledge of magnetic fields can lead to at most an order of magnitude changes in the predicted synchrotron fluxes.

C. Constraints on $\langle\sigma v\rangle$ - m

1. Constraint from the measurement at 330 MHz

In the region with radius 2° around the GC, data in the 330 MHz radio band is presented in [83]. We compare our prediction of the synchrotron flux from products

of DM annihilation, and demand that the radio is not over-saturated by the DM-induced fluxes. This gives us a constraint on the DM annihilation cross section $\langle\sigma v\rangle \sim 10^{-25} \text{cm}^3 \text{s}^{-1}$. This is overly conservative, as there are known astrophysical sources that produce most of the observed synchrotron radiation. The astrophysical model presented in [83] suggests that with present level of uncertainty, at most 5% of the flux ($\lesssim 900 \text{Jy}$) could come from unknown sources. This gives a much stronger constraint $\langle\sigma v\rangle \lesssim 10^{-26} \text{cm}^3 \text{s}^{-1}$. This constraint on the $\langle\sigma v\rangle$ - m plane that can be derived from the radio flux measurement at 330 MHz for a circular region of radius 2° is plotted in the top panel of Fig. 4. We only show the constraints that can be obtained in this radio band by using the exponential magnetic field given in Eq. (17), with a normalization of $6 \mu\text{G}$.

For both the DM self annihilation channels $\chi\chi \rightarrow Z\gamma$ and $\chi\chi \rightarrow H\gamma$, we see that the contracted NFW profile gives the most constraining limit. Since the gamma-ray line prefers a cross section $\langle\sigma v\rangle \sim 10^{-27} \text{cm}^3 \text{s}^{-1}$ for all the three profiles [14], it can be concluded that the existing data at this frequency is not able to constrain the line signal independent of a DM particle physics model. However, since the present constraints are only an order of magnitude away from the DM self annihilation cross section preferred by the 130 GeV signal, a future radio measurement near the GC can be used to either constrain or confirm its presence at the GC.

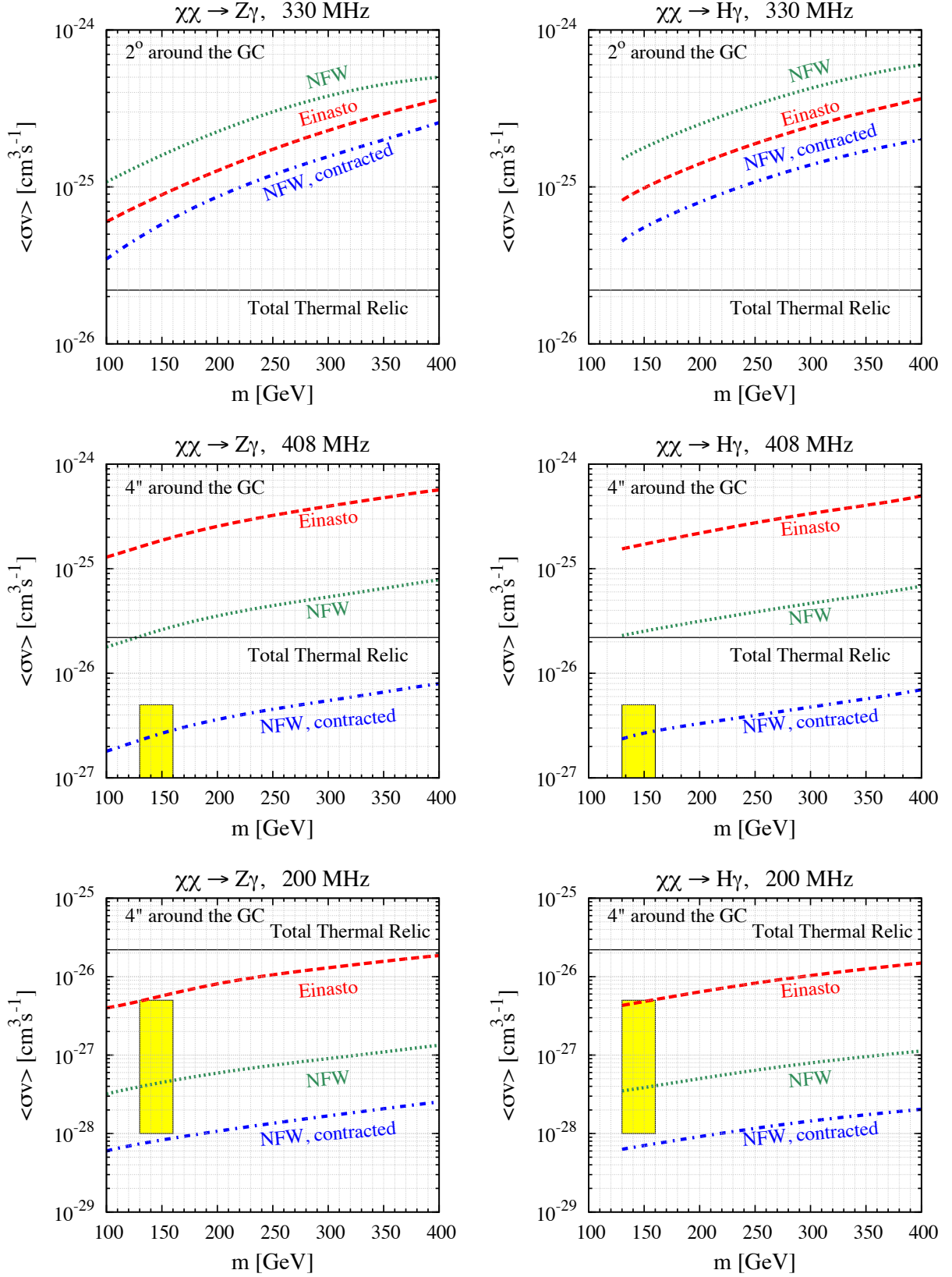


FIG. 4. Constraints obtained in the $\langle\sigma v\rangle$ vs. m plane for different annihilation channels, different frequency bands, and different regions of observations. In all the plots, three different DM profiles are considered: Einasto profile Eq. (14), NFW profile Eq. (15) and the contracted NFW profile Eq. (16). **(Left)** $\chi\chi \rightarrow Z\gamma$. **(Right)** $\chi\chi \rightarrow H\gamma$. **(Top)** The results are for 330 MHz using the exponential magnetic field in Eq. (17). **(Middle)** The results are for 408 MHz using the equipartition magnetic field in Eq. (18). **(Bottom)** The results are for 200 MHz using the equipartition magnetic field in Eq. (18). All magnetic fields used in this figure have been normalized to be $6 \mu\text{G}$ at the solar radius. The shaded region shows approximately the region favored by the recent 130 GeV gamma-ray line signal [14]. We also show the updated total thermal relic cross section for reference [116].

2. Constraint from the measurement at 408 MHz

The upper-limit on the synchrotron flux at 408 MHz found by [84] allows us to impose much stronger constraints than above. The procedure that we follow is similar to above - we compare the predicted fluxes with the existing upper limit, and demand that the DM annihilation not produce a flux larger than what is already constrained. This constraint in the $\langle\sigma v\rangle$ - m plane that can be derived from the radio flux measurement at 408 MHz for a circular region of radius $4''$ is plotted in the second row of Fig. 4. For both the DM self annihilation channels $\chi\chi \rightarrow Z\gamma$ and $\chi\chi \rightarrow H\gamma$, we see again that the contracted NFW profile gives the most constraining limit ($\langle\sigma v\rangle \lesssim 10^{-27} \text{ cm}^3 \text{ s}^{-1}$), and in fact the sensitivity to the cross section is less than the total thermal relic cross section for both the self annihilation channels. The least constraining limit is obtained from the Einasto DM profile, as expected ($\langle\sigma v\rangle \lesssim 10^{-25} \text{ cm}^3 \text{ s}^{-1}$). If we trust the modeling of the magnetic field near the GC black hole, then this shows that the interpretation of the line signal near the GC for a contracted NFW profile is in mild tension with the radio data, provided the source of the gamma-ray line in the GC is due to the $\chi\chi \rightarrow Z\gamma$ and $\chi\chi \rightarrow H\gamma$ self annihilation channel.

3. Sensitivity from a future measurement at 200 MHz

The situation is expected to improve dramatically with LOFAR observation at lower frequencies. To forecast the sensitivity, we assume that LOFAR can reach a flux density of 3.2 mJy at 200 MHz for a circular region of radius $4''$ around the GC. This expectation stems from [82], where we see that LOFAR can reach arc-second angular resolution and can probe down to 0.2 mJy fluxes near the GC. For a region of interest $4''$ around the GC, we then deduce the sensitivity that can be reached by LOFAR as 3.2 mJy.

The constraint in the $\langle\sigma v\rangle$ - m plane that can be derived from the radio flux measurement at 200 MHz for a circular region of radius $4''$ is plotted in Fig. 4. Due to the superior flux sensitivity of LOFAR at these frequencies, we see that both the $\chi\chi \rightarrow Z\gamma$ and $\chi\chi \rightarrow H\gamma$ self annihilation channel can be probed well below the total thermal relic cross section for all three considered DM profiles. In particular, for both NFW and contracted NFW profiles, one can probe below the $\langle\sigma v\rangle \sim 10^{-27} \text{ cm}^3 \text{ s}^{-1}$ cross sections required to test the tentative 130 GeV signal. Thus, if the 130 GeV gamma-ray line turns out to be robust and originates from DM self annihilation, LOFAR has a good chance to search for the self annihilation channel giving rise to the line for both the NFW and the contracted NFW profile. Up to the uncertainty in the GC model, this remains, to our knowledge, the best probe for discerning the origin of the DM line independent of any particle physics DM model. We remind the readers that LOFAR can reach

this sensitivity in 6 hours of observation of the GC, and longer time of observation will only strengthen our result. Also an observation by LOFAR over a larger region of observation will decrease the dependence on the DM profile and may provide more robust results.

V. SUMMARY AND OUTLOOK

In this paper we have shown that existing radio data around the Galactic Center at 408 MHz marginally constrains the interpretation of the 130 GeV line in Fermi-LAT data in terms of DM self annihilation to $Z\gamma$ or $H\gamma$ with a cross section $\sim 10^{-27} \text{ cm}^3 \text{ s}^{-1}$ for a contracted NFW profile. For other frequencies or other DM density profiles the constraint is weaker by about an order of magnitude. Future measurements made around the GC by LOFAR in the 200 MHz band can push the sensitivity to DM annihilating to gamma-ray lines down by an order of magnitude to $\langle\sigma v\rangle \sim 10^{-28} \text{ cm}^3 \text{ s}^{-1}$ and enable a test of the above signal for both the NFW and the contracted NFW density profile. These possibilities are, to the best of our knowledge, some of the most competitive ways to test for the nature of the DM that could have produced the tentative 130 GeV line signal.

We have shown that these conclusions are fairly robust with respect to the assumptions on the magnetic field in the Galaxy, and the constraints do not weaken by more than an order of magnitude. The dependence on DM density profiles is somewhat more important, especially when the region of observation is small and closely centered on the GC. While the uncertainty in the astrophysical modeling of the GC does impact our results, we must emphasize that these constraints are completely model-independent from the particle physics perspective, because we have simply taken the electrons and positrons from the known decays of the Z or H produced in the DM annihilation to $Z\gamma$ or $H\gamma$, respectively.

We hope that these results will encourage radio astronomers, especially those at LOFAR and SKA, to observe the GC, model the astrophysical synchrotron backgrounds, and determine if there is any excess flux. Irrespective of whether the tentative 130 GeV gamma-ray line signal at Fermi-LAT is due to DM annihilation or not, this promises to deliver some of the strongest constraints on DM annihilation.

ACKNOWLEDGMENTS

We thank John Beacom, Sayan Chakraborti, Christopher Kochanek, Kohta Murase, Brian Lacki, and Todd Thompson for helpful discussions. B.D. and R.L. also thank Ilias Cholis, Alex Geringer-Sameth, Joachim Kopp, Tim Linden, Marco Taoso, Douglas Spolyar, and Christoph Weniger for interesting questions and suggestions at the IDM 2012 conference where this work

was first presented. R.L. is supported by NSF grant PHY-1101216 awarded to John Beacom.

-
- [1] G. Jungman, M. Kamionkowski, and K. Griest, “Supersymmetric dark matter”, *Phys. Rept.* **267** (1996) 195–373, [arXiv:hep-ph/9506380](#).
- [2] G. Bertone, D. Hooper, and J. Silk, “Particle dark matter: Evidence, candidates and constraints”, *Phys. Rept.* **405** (2005) 279–390, [arXiv:hep-ph/0404175](#).
- [3] L. Bergstrom, “Saas-Fee Lecture Notes: Multi-messenger Astronomy and Dark Matter”, [arXiv:1202.1170](#).
- [4] J. L. Feng, “Dark Matter Candidates from Particle Physics and Methods of Detection”, *Ann.Rev.Astron.Astrophys.* **48** (2010) 495–545, [arXiv:1003.0904](#).
- [5] J. Gunn, B. Lee, I. Lerche, D. Schramm, and G. Steigman, “Some Astrophysical Consequences of the Existence of a Heavy Stable Neutral Lepton”, *Astrophys.J.* **223** (1978) 1015–1031.
- [6] L. Bergstrom and H. Snellman, “Observable monochromatic photons from cosmic photino annihilation”, *Phys.Rev.* **D37** (1988) 3737–3741.
- [7] R. Flores, K. A. Olive, and S. Rudaz, “Radiative processes in LSP annihilation”, *Phys.Lett.* **B232** (1989) 377–382.
- [8] L. Bergstrom and P. Ullio, “Full one loop calculation of neutralino annihilation into two photons”, *Nucl.Phys.* **B504** (1997) 27–44, [arXiv:hep-ph/9706232](#).
- [9] Z. Bern, P. Gondolo, and M. Perelstein, “Neutralino annihilation into two photons”, *Phys.Lett.* **B411** (1997) 86–96, [arXiv:hep-ph/9706538](#).
- [10] P. Ullio and L. Bergstrom, “Neutralino annihilation into a photon and a Z boson”, *Phys.Rev.* **D57** (1998) 1962–1971, [arXiv:hep-ph/9707333](#).
- [11] G. Bertone, C. Jackson, G. Shaughnessy, T. M. Tait, and A. Vallinotto, “The WIMP Forest: Indirect Detection of a Chiral Square”, *Phys.Rev.* **D80** (2009) 023512, [arXiv:0904.1442](#).
- [12] CMS Collaboration, S. Chatrchyan *et al.*, “Observation of a new boson at a mass of 125 GeV with the CMS experiment at the LHC”, *Phys.Lett.B*, 2012 [arXiv:1207.7235](#).
- [13] ATLAS Collaboration, G. Aad *et al.*, “Observation of a new particle in the search for the Standard Model Higgs boson with the ATLAS detector at the LHC”, [arXiv:1207.7214](#).
- [14] C. Weniger, “A Tentative Gamma-Ray Line from Dark Matter Annihilation at the Fermi Large Area Telescope”, [arXiv:1204.2797](#).
- [15] T. Bringmann, X. Huang, A. Ibarra, S. Vogl, and C. Weniger, “Fermi LAT Search for Internal Bremsstrahlung Signatures from Dark Matter Annihilation”, [arXiv:1203.1312](#).
- [16] E. Tempel, A. Hektor, and M. Raidal, “Fermi 130 GeV gamma-ray excess and dark matter annihilation in sub-halos and in the Galactic centre”, [arXiv:1205.1045](#).
- [17] A. Boyarsky, D. Malyshev, and O. Ruchayskiy, “Spectral and spatial variations of the diffuse gamma-ray background in the vicinity of the Galactic plane and possible nature of the feature at 130 GeV”, [arXiv:1205.4700](#).
- [18] A. Rajaraman, T. M. Tait, and D. Whiteson, “Two Lines or Not Two Lines? That is the Question of Gamma Ray Spectra”, [arXiv:1205.4723](#).
- [19] A. Geringer-Sameth and S. M. Koushiappas, “Dark matter line search using a joint analysis of dwarf galaxies with Fermi”, [arXiv:1206.0796](#).
- [20] M. Su and D. P. Finkbeiner, “Strong Evidence for Gamma-ray Line Emission from the Inner Galaxy”, [arXiv:1206.1616](#).
- [21] W. Buchmuller and M. Garny, “Decaying vs Annihilating Dark Matter in Light of a Tentative Gamma-Ray Line”, [arXiv:1206.7056](#).
- [22] T. Cohen, M. Lisanti, T. R. Slatyer, and J. G. Wacker, “Illuminating the 130 GeV Gamma Line with Continuum Photons”, [arXiv:1207.0800](#).
- [23] I. Cholis, M. Tavakoli, and P. Ullio, “Searching for the continuum spectrum photons correlated to the 130 GeV gamma-ray line”, [arXiv:1207.1468](#).
- [24] M. Su and D. P. Finkbeiner, “Double Gamma-ray Lines from Unassociated Fermi-LAT Sources”, [arXiv:1207.7060](#).
- [25] L. Bergstrom, G. Bertone, J. Conrad, C. Farnier, and C. Weniger, “Investigating Gamma-Ray Lines from Dark Matter with Future Observatories”, [arXiv:1207.6773](#).
- [26] A. Hektor, M. Raidal, and E. Tempel, “An evidence for indirect detection of dark matter from galaxy clusters in Fermi-LAT data”, [arXiv:1207.4466](#).
- [27] R.-Z. Yang, Q. Yuan, L. Feng, Y.-Z. Fan, and J. Chang, “Statistical interpretation of the spatial distribution of current 130 GeV gamma-ray line signal within the dark matter annihilation scenario”, [arXiv:1207.1621](#).
- [28] X.-Y. Huang, Q. Yuan, P.-F. Yin, X.-J. Bi, and X.-L. Chen, “Constraints on the dark matter annihilation scenario of Fermi 130 GeV γ -ray line emission by continuous gamma-rays, Milky Way halo, galaxy clusters and dwarf galaxies observations”, [arXiv:1208.0267](#).
- [29] L. Feng, Q. Yuan, and Y.-Z. Fan, “Tentative wiggle in the cosmic ray electron/positron spectrum at ~ 100 GeV: a dark matter annihilation signal in accordance with the 130 GeV γ -ray line?”, [arXiv:1206.4758](#).
- [30] Y. Li and Q. Yuan, “Testing the 130 GeV gamma-ray line with high energy resolution detectors”, [arXiv:1206.2241](#).
- [31] D. Whiteson, “Disentangling Instrumental Features of the 130 GeV Fermi Line”, [arXiv:1208.3677](#).
- [32] Fermi-LAT Collaboration, M. Ackermann *et al.*, “Fermi LAT Search for Dark Matter in Gamma-ray Lines and the Inclusive Photon Spectrum”, [arXiv:1205.2739](#).
- [33] A. Ibarra, S. Lopez Gehler, and M. Pato, “Dark matter constraints from box-shaped gamma-ray features”, [arXiv:1205.0007](#).

- [34] E. Dudas, Y. Mambrini, S. Pokorski, and A. Romagnoni, “Extra U(1) as natural source of a monochromatic gamma ray line”, [arXiv:1205.1520](#).
- [35] J. M. Cline, “130 GeV dark matter and the Fermi gamma-ray line”, [arXiv:1205.2688](#).
- [36] K.-Y. Choi and O. Seto, “A Dirac right-handed sneutrino dark matter and its signature in the gamma-ray lines”, [arXiv:1205.3276](#).
- [37] B. Kyae and J.-C. Park, “130 GeV Gamma-Ray Line from Dark Matter Decay”, [arXiv:1205.4151](#).
- [38] H. M. Lee, M. Park, and W.-I. Park, “Fermi Gamma Ray Line at 130 GeV from Axion-Mediated Dark Matter”, [arXiv:1205.4675](#).
- [39] B. S. Acharya, G. Kane, P. Kumar, R. Lu, and B. Zheng, “Mixed Wino-Axion Dark Matter in String/M Theory and the 130 GeV Gamma-line ‘Signal’”, [arXiv:1205.5789](#).
- [40] M. R. Buckley and D. Hooper, “Implications of a 130 GeV Gamma-Ray Line for Dark Matter”, [arXiv:1205.6811](#).
- [41] X. Chu, T. Hambye, T. Scarna, and M. H. Tytgat, “What if Dark Matter Gamma-Ray Lines come with Gluon Lines?”, [arXiv:1206.2279](#).
- [42] D. Das, U. Ellwanger, and P. Mitropoulos, “A 130 GeV photon line from dark matter annihilation in the NMSSM”, [arXiv:1206.2639](#).
- [43] Z. Kang, T. Li, J. Li, and Y. Liu, “Brightening the (130 GeV) Gamma-Ray Line”, [arXiv:1206.2863](#).
- [44] N. Weiner and I. Yavin, “How Dark Are Majorana WIMPs? Signals from MiDM and Rayleigh Dark Matter”, [arXiv:1206.2910](#).
- [45] J. H. Heo and C. Kim, “Cosmic ray signatures of Dipole-Interacting Fermionic Dark Matter”, [arXiv:1207.1341](#).
- [46] S. Tulin, H.-B. Yu, and K. M. Zurek, “Three Exceptions for Thermal Dark Matter with Enhanced Annihilation to Gamma Gamma”, [arXiv:1208.0009](#).
- [47] T. Li, J. A. Maxin, D. V. Nanopoulos, and J. W. Walker, “A 125.5 GeV Higgs Boson in F-SU(5): Imminently Observable Proton Decay, A 130 GeV Gamma-ray Line, and SUSY Multijets and Light Stops at the LHC8”, [arXiv:1208.1999](#).
- [48] J.-C. Park and S. C. Park, “Radiatively decaying scalar dark matter through U(1) mixings and the Fermi 130 GeV gamma-ray line”, [arXiv:1207.4981](#).
- [49] M. T. Frandsen, U. Haisch, F. Kahlhoefer, P. Mertsch, and K. Schmidt-Hoberg, “Loop-induced dark matter direct detection signals from gamma-ray lines”, [arXiv:1207.3971](#).
- [50] I. Oda, “Remarks on Two Gamma Ray Lines from the Inner Galaxy”, [arXiv:1207.1537](#).
- [51] J. M. Cline, A. R. Frey, and G. D. Moore, “Composite magnetic dark matter and the 130 GeV line”, [arXiv:1208.2685](#).
- [52] Y. Bai and J. Shelton, “Gamma Lines without a Continuum: Thermal Models for the Fermi-LAT 130 GeV Gamma Line”, [arXiv:1208.4100](#).
- [53] M. Kuhlen, J. Guedes, A. Pillepich, P. Madau, and L. Mayer, “An Off-center Density Peak in the Milky Way’s Dark Matter Halo?”, [arXiv:1208.4844](#).
- [54] S. Profumo and T. Linden, “Gamma-ray Lines in the Fermi Data: is it a Bubble?”, [arXiv:1204.6047](#).
- [55] F. Aharonian, D. Khangulyan, and D. Malyshev, “Cold ultrarelativistic pulsar winds as potential sources of galactic gamma-ray lines above 100 GeV”, [arXiv:1207.0458](#).
- [56] D. Hooper and T. Linden, “Are Lines From Unassociated Gamma-Ray Sources Evidence For Dark Matter Annihilation?”, [arXiv:1208.0828](#).
- [57] N. Mirabal, “The Dark Knight Falterers”, [arXiv:1208.1693](#).
- [58] A. Hektor, M. Raidal, and E. Tempel, “Double gamma-ray lines from unassociated Fermi-LAT sources revisited”, [arXiv:1208.1996](#).
- [59] **PAMELA** Collaboration, O. Adriani *et al.*, “An anomalous positron abundance in cosmic rays with energies 1.5-100 GeV”, *Nature* **458** (2009) 607–609, [arXiv:0810.4995](#).
- [60] **Fermi-LAT** Collaboration, M. Ackermann *et al.*, “Measurement of separate cosmic-ray electron and positron spectra with the Fermi Large Area Telescope”, *Phys.Rev.Lett.* **108** (2012) 011103, [arXiv:1109.0521](#).
- [61] **IceCube** Collaboration, R. Abbasi *et al.*, “Search for Dark Matter from the Galactic Halo with the IceCube Neutrino Observatory”, *Phys.Rev.* **D84** (2011) 022004, [arXiv:1101.3349](#).
- [62] J. F. Beacom, N. F. Bell, and G. D. Mack, “General Upper Bound on the Dark Matter Total Annihilation Cross Section”, *Phys.Rev.Lett.* **99** (2007) 231301, [arXiv:astro-ph/0608090](#).
- [63] H. Yuksel, S. Horiuchi, J. F. Beacom, and S. Ando, “Neutrino Constraints on the Dark Matter Total Annihilation Cross Section”, *Phys.Rev.* **D76** (2007) 123506, [arXiv:0707.0196](#).
- [64] B. Dasgupta and R. Laha, “Neutrinos in IceCube/KM3NeT as probes of Dark Matter Substructures in Galaxy Clusters”, [arXiv:1206.1322](#).
- [65] R. Aloisio, P. Blasi, and A. V. Olinto, “Neutralino annihilation at the Galactic Center revisited”, *JCAP* **0405** (2004) 007, [arXiv:astro-ph/0402588](#).
- [66] E. Borriello, A. Cuoco, and G. Miele, “Radio constraints on dark matter annihilation in the galactic halo and its substructures”, *Phys.Rev.* **D79** (2009) 023518, [arXiv:0809.2990](#).
- [67] G. Bertone, M. Cirelli, A. Strumia, and M. Taoso, “Gamma-ray and radio tests of the e+e- excess from DM annihilations”, *JCAP* **0903** (2009) 009, [arXiv:0811.3744](#).
- [68] K. Ishiwata, S. Matsumoto, and T. Moroi, “Synchrotron Radiation from the Galactic Center in Decaying Dark Matter Scenario”, *Phys.Rev.* **D79** (2009) 043527, [arXiv:0811.4492](#).
- [69] N. Fornengo, R. A. Lineros, M. Regis, and M. Taoso, “Galactic synchrotron emission from WIMPs at radio frequencies”, *JCAP* **1201** (2012) 005, [arXiv:1110.4337](#).
- [70] R. Crocker, N. Bell, C. Balazs, and D. Jones, “Radio and gamma-ray constraints on dark matter annihilation in the Galactic center”, *Phys.Rev.* **D81** (2010) 063516, [arXiv:1002.0229](#).
- [71] P. Gondolo, “Either neutralino dark matter or cuspy dark halos”, *Phys.Lett.* **B494** (2000) 181–186, [arXiv:hep-ph/0002226](#).
- [72] L. Bergstrom, G. Bertone, T. Bringmann, J. Edsjo, and M. Taoso, “Gamma-ray and Radio Constraints of High Positron Rate Dark Matter Models Annihilating into New Light Particles”, *Phys.Rev.* **D79** (2009) 081303, [arXiv:0812.3895](#).

- [73] D. Hooper, D. P. Finkbeiner, and G. Dobler, “Possible evidence for dark matter annihilations from the excess microwave emission around the center of the Galaxy seen by the Wilkinson Microwave Anisotropy Probe”, *Phys.Rev.* **D76** (2007) 083012, [arXiv:0705.3655](#).
- [74] M. Regis and P. Ullio, “Multi-wavelength signals of dark matter annihilations at the Galactic center”, *Phys.Rev.* **D78** (2008) 043505, [arXiv:0802.0234](#).
- [75] G. Bertone, G. Sigl, and J. Silk, “Astrophysical limits on massive dark matter”, *Mon.Not.Roy.Astron.Soc.* **326** (2001) 799–804, [arXiv:astro-ph/0101134](#).
- [76] D. Hooper and T. Linden, “Gamma Rays From The Galactic Center and the WMAP Haze”, *Phys.Rev.* **D83** (2011) 083517, [arXiv:1011.4520](#).
- [77] D. Hooper, A. V. Belikov, T. E. Jeltema, T. Linden, S. Profumo, *et al.*, “The Isotropic Radio Background and Annihilating Dark Matter”, [arXiv:1203.3547](#).
- [78] N. Fornengo, R. Lineros, M. Regis, and M. Taoso, “Possibility of a Dark Matter Interpretation for the Excess in Isotropic Radio Emission Reported by ARCADE”, *Phys.Rev.Lett.* **107** (2011) 271302, [arXiv:1108.0569](#).
- [79] L. Zhang, J. Redondo, and G. Sigl, “Galactic Signatures of Decaying Dark Matter”, *JCAP* **0909** (2009) 012, [arXiv:0905.4952](#).
- [80] L. Zhang and G. Sigl, “Dark Matter Signatures in the Anisotropic Radio Sky”, *JCAP* **0809** (2008) 027, [arXiv:0807.3429](#).
- [81] Y. Mambrini, M. H. Tytgat, G. Zaharijas, and B. Zaldivar, “Complementarity of Galactic radio and collider data in constraining WIMP dark matter models”, [arXiv:1206.2352](#).
- [82] N. E. Kassim, T. J. W. Lazio, M. Nord, S. D. Hyman, C. L. Brogan, T. N. Larosa, and N. Duric, “Prospects for LOFAR Observations of the Galactic Center”, *Astronomische Nachrichten Supplement* **324** (2003) 65–71.
- [83] R. M. Crocker, D. I. Jones, F. Melia, J. Ott, and R. J. Protheroe, “A lower limit of 50 microgauss for the magnetic field near the Galactic Centre”, *Nature (London)* **463** (2010) 65–67, [arXiv:1001.1275](#).
- [84] R. D. Davies, D. Walsh, and R. S. Booth, “The radio source at the galactic nucleus”, *Mon.Not.Roy.Astron.Soc.* **177** (1976) 319–333.
- [85] E. Wommer, F. Melia, and M. Fatuzzo, “Diffuse TeV Emission at the Galactic Centre”, [arXiv:0804.3111](#).
- [86] **Particle Data Group** Collaboration, K. Nakamura *et al.*, “Review of particle physics”, *J.Phys.G* **G37** (2010) 075021.
- [87] M. S. Longair, “High Energy Astrophysics”, 2010.
- [88] T. Sjostrand, S. Mrenna, and P. Z. Skands, “A Brief Introduction to PYTHIA 8.1”, *Comput.Phys.Commun.* **178** (2008) 852–867, [arXiv:0710.3820](#).
- [89] G. B. Rybicki and A. P. Lightman, “Radiative Processes in Astrophysics”, 1986.
- [90] A. E. Schulz, R. Mandelbaum, and N. Padmanabhan, “Testing adiabatic contraction with Sloan Digital Sky Survey elliptical galaxies”, *Mon.Not.Roy.Astron.Soc.* **408** (2010) 1463–1475, [arXiv:0911.2260](#).
- [91] M. W. Auger, T. Treu, R. Gavazzi, A. S. Bolton, L. V. E. Koopmans, and P. J. Marshall, “Dark Matter Contraction and the Stellar Content of Massive Early-type Galaxies: Disfavoring ”Light” Initial Mass Functions”, *Astrophysical Journal Letters* **721** (2010) L163–L167, [arXiv:1007.2409](#).
- [92] M. S. Seigar, A. J. Barth, and J. S. Bullock, “A revised Λ CDM mass model for the Andromeda Galaxy”, *Mon.Not.Roy.Astron.Soc.* **389** (2008) 1911–1923, [arXiv:astro-ph/0612228](#).
- [93] N. R. Napolitano, A. J. Romanowsky, M. Capaccioli, N. G. Douglas, M. Arnaboldi, L. Coccatto, O. Gerhard, K. Kuijken, M. R. Merrifield, S. P. Bamford, A. Cortesi, P. Das, and K. C. Freeman, “The PN.S Elliptical Galaxy Survey: a standard Λ CDM halo around NGC 4374?”, *Mon.Not.Roy.Astron.Soc.* **411** (2011) 2035–2053, [arXiv:1010.1533](#).
- [94] O. Y. Gnedin, D. Ceverino, N. Y. Gnedin, A. A. Klypin, A. V. Kravtsov, *et al.*, “Halo Contraction Effect in Hydrodynamic Simulations of Galaxy Formation”, [arXiv:1108.5736](#).
- [95] W. de Blok, “The Core-Cusp Problem”, *Adv.Astron.* **2010** (2010) 789293, [arXiv:0910.3538](#).
- [96] J. Bovy and S. Tremaine, “On the local dark matter density”, [arXiv:1205.4033](#).
- [97] R. Catena and P. Ullio, “A novel determination of the local dark matter density”, *JCAP* **1008** (2010) 004, [arXiv:0907.0018](#).
- [98] P. Salucci, F. Nesti, G. Gentile, and C. Martins, “The dark matter density at the Sun’s location”, *Astron.Astrophys.* **523** (2010) A83, [arXiv:1003.3101](#).
- [99] J. Einasto, “On the Construction of a Composite Model for the Galaxy and on the Determination of the System of Galactic Parameters”, *Trudy Astrofizicheskogo Instituta Alma-Ata* **5** (1965) 87–100.
- [100] J. F. Navarro, E. Hayashi, C. Power, A. Jenkins, C. S. Frenk, *et al.*, “The Inner structure of Lambda-CDM halos 3: Universality and asymptotic slopes”, *Mon.Not.Roy.Astron.Soc.* **349** (2004) 1039, [arXiv:astro-ph/0311231](#).
- [101] V. Springel, J. Wang, M. Vogelsberger, A. Ludlow, A. Jenkins, *et al.*, “The Aquarius Project: the subhalos of galactic halos”, *Mon.Not.Roy.Astron.Soc.* **391** (2008) 1685–1711, [arXiv:0809.0898](#).
- [102] L. Pieri, J. Lavalle, G. Bertone, and E. Branchini, “Implications of High-Resolution Simulations on Indirect Dark Matter Searches”, *Phys.Rev.* **D83** (2011) 023518, [arXiv:0908.0195](#).
- [103] J. F. Navarro, C. S. Frenk, and S. D. White, “A Universal density profile from hierarchical clustering”, *Astrophys.J.* **490** (1997) 493–508, [arXiv:astro-ph/9611107](#).
- [104] P. Gondolo and J. Silk, “Dark matter annihilation at the galactic center”, *Phys.Rev.Lett.* **83** (1999) 1719–1722, [arXiv:astro-ph/9906391](#).
- [105] G. R. Blumenthal, S. Faber, R. Flores, and J. R. Primack, “Contraction of Dark Matter Galactic Halos Due to Baryonic Infall”, *Astrophys.J.* **301** (1986) 27.
- [106] B. S. Ryden and J. E. Gunn, “Galaxy formation by gravitational collapse”, *Astrophys. J.* **318** (1987) 15–31.
- [107] O. Y. Gnedin and J. R. Primack, “Dark Matter Profile in the Galactic Center”, *Phys.Rev.Lett.* **93** (2004) 061302, [arXiv:astro-ph/0308385](#).
- [108] M. Gustafsson, M. Fairbairn, and J. Sommer-Larsen, “Baryonic Pinching of Galactic Dark Matter Haloes”, *Phys.Rev.* **D74** (2006) 123522, [arXiv:astro-ph/0608634](#).

- [109] F. Iocco, M. Pato, G. Bertone, and P. Jetzer, “Dark Matter distribution in the Milky Way: microlensing and dynamical constraints”, *JCAP* **1111** (2011) 029, [arXiv:1107.5810](#).
- [110] T. LaRosa, C. Brogan, S. Shore, T. Lazio, N. Kassim, *et al.*, “Evidence for a weak Galactic Center magnetic field from diffuse low frequency nonthermal radio emission”, *Astrophys.J.* **626** (2005) L23–L28, [arXiv:astro-ph/0505244](#).
- [111] M. Morris and F. Yusef-Zadeh, “The thermal, arched filaments of the radio arc near the Galactic center - Magnetohydrodynamic-induced ionization?”, *Astrophys. J.* **343** (1989) 703–712.
- [112] J. Han, R. Manchester, A. Lyne, G. Qiao, and W. van Straten, “Pulsar rotation measures and the large-scale structure of Galactic magnetic field”, *Astrophys.J.* **642** (2006) 868–881, [arXiv:astro-ph/0601357](#).
- [113] R. Jansson, G. R. Farrar, A. H. Waelkens, and T. A. Ensslin, “Constraining models of the large scale Galactic magnetic field with WMAP5 polarization data and extragalactic Rotation Measure sources”, *JCAP* **0907** (2009) 021, [arXiv:0905.2228](#).
- [114] M. Pshirkov, P. Tinyakov, P. Kronberg, and K. Newton-McGee, “Deriving global structure of the Galactic Magnetic Field from Faraday Rotation Measures of extragalactic sources”, *Astrophys.J.* **738** (2011) 192, [arXiv:1103.0814](#).
- [115] L. Bergstrom, M. Fairbairn, and L. Pieri, “X-ray Radiation from the Annihilation of Dark Matter at the Galactic Center”, *Phys.Rev.* **D74** (2006) 123515, [arXiv:astro-ph/0607327](#).
- [116] G. Steigman, B. Dasgupta, and J. F. Beacom, “Precise Relic WIMP Abundance and its Impact on Searches for Dark Matter Annihilation”, *Phys.Rev.* **D86** (2012) 023506, [arXiv:1204.3622](#).